A versatile model of steady state O_2 supply to tissue

Application to skeletal muscle

K. Groebe

Institut für Physiologie und Pathophysiologie, Johannes Gutenberg-Universität Mainz, Saarstrasse 21, D-6500 Mainz, West Germany

ABSTRACT A model of combined convective and diffusive O_2 transport to tissue is suggested which allows for the calculation of P_{O_2} distributions in a cuboid tissue region with arbitrary microvascular geometries and blood flows. Carrier-facilitated O_2 diffusion in the erythrocytes and in the tissue and red blood cell reaction kinetics are considered. The model is based on analytical descriptions of the P_{O_2} fields of single erythrocytes surrounded by carrier-free layers in an infinite three-dimensional space containing an O_2 carrier such as myoglobin. These P_{O_2} fields are overlaid to obtain a solution of the differential equation of diffusion in respiring tissue.

The model has been applied to a situation in heavily working skeletal muscle. Resulting P_{O_2} profiles exhibit steep peri-capillary P_{O_2} gradients. Further into the fiber, the profiles are essentially flat at low P_{O_2} levels in good agreement with experimental findings (Gayeski and Honig. 1986. *Am. J. Physiol.* 251:H789–H799). P_{O_2} dependence of facilitation of O_2 transport produces a "layer deficient of functional carrier" which extends into the muscle fiber and which represents a reserve of O_2 conductance automatically recruited in exercise. Furthermore, it results in a homogenization of red blood cell O_2 fluxes which accounts for the absence of P_{O_2} gradients along the muscle fiber axis (cf. Gayeski and Honig. 1988. *Am. J. Physiol.* 254: H1179–H1186).

INTRODUCTION

During the past years it has been recognized that heterogeneities in vascular geometry and blood flows have important impacts on O_2 transport to tissue which cannot be appreciated by considering solely the mean values of capillary density, capillary length, and capillary flow. Therefore, a number of efforts have been made to gain more quantitative information on microvessel architecture and flows. Distributions of capillary length, density, and blood flow, and of red blood cell (RBC) flow path lengths and transit times have been reported for various skeletal muscles (Egginton et al., 1987; Honig et al., 1977; Honig and Odoroff, 1981; Sarelius, 1986). Moreover, directions of flow and staggering of capillaries in heart muscle have been investigated (Reeves and Rakusan, 1987).

In order to incorporate this expanding information into mathematical descriptions of tissue oxygenation, more flexible models need to be developed. One approach aiming in this direction (Groebe and Thews, 1986) allows for the calculation of three-dimensional P_{O_2} profiles in cylindrical muscle fibers with arbitrary distributions of RBCs on their surface. Two more recent studies (Clark et al., 1989; Hoofd et al., 1989) describe the P_{O_2} profiles in a plane perpendicular to the capillary direction for an arbitrary arrangement of capillary cross sections in this plane.

The major shortcoming of models that do not incorporate RBC desaturation along the capillaries is that phenomena such as dispersion of capillary density, lengths, flows, or transit times, counter current flow, or staggering of capillary origins cannot be taken into account appropriately. On the other hand, models that consider complex capillary geometries and include capillary O_2 desaturation (e.g., Grunewald and Sowa, 1977; Popel, 1980) typically are restricted to very special geometrical arrangements for reasons of analytical or numerical tractability.

The tissue O_2 supply model suggested in this paper brings together a number of features of which only one or the other were considered in former models: (*a*) three-dimensional calculations; (*b*) arbitrary capillary geometry; (*c*) arbitrary RBC flux distribution; (*d*) arbitrary RBC velocity distribution; (*e*) effects of the particulate nature of blood; (*f*) RBC O_2 desaturation along the capillary; (*g*) plain and hemoglobin (Hb)-facilitated O_2 diffusion and reaction kinetics inside RBCs; (*h*) plain and myoglobin (Mb)-facilitated O_2 diffusion inside the tissue; and (*i*) carrier-free layer separating RBC and tissue. As an application, P_{O_2} distributions in maximally working skeletal muscle are calculated. The resulting profiles shed some light on the reserve of muscle O_2 conductance, which allows for a 50–100-fold increase in O_2 flux in rest-work transition.

ANALYSIS

Approach

The basic element of the model is an analytical description of the P_{O_2} field of a single erythrocyte with a given O_2 saturation, surrounded by a carrier-free layer in an infinite three-dimensional space which contains an O_2 carrier such as myoglobin. P_{O_2} drops due to intra-erythrocytic plain and Hb-facilitated O_2 diffusion and to Hb-O_2-reaction kinetics are considered according to Clark et al., (1985) and Clark and Clark (1986). In addition to the RBC O_2 saturation, each of these P_{O_2} fields still contains the O_2 flux out of the RBC as unknown, because P_{O_2} at the interface between carrier-free layer and tissue cannot be matched for an individual one of these particular solutions separately since Mb saturation depends on the absolute value of P_{O_2}. By overlaying these basic elements for all RBCs positioned at arbitrary locations in the tissue region considered, and by adding a term that accounts for O_2 consumption in this region, one obtains a solution of the differential equation of diffusion in respiring tissue. Matching P_{O_2} at all of the interfaces between carrier-free layers and tissue and adjusting overall RBC O_2 fluxes to a prescribed O_2 consumption rate results in a large, nonlinear system of equations with the RBC O_2 saturations and O_2 fluxes as unknowns. For a given set of RBC O_2 fluxes, this system of equations is explicit in the RBC O_2 saturations: If the saturations of in- or outflowing RBCs are prescribed, the other saturations may be calculated from RBC O_2 fluxes and RBC velocities. (RBC velocities may be obtained from a hemodynamic model of microvascular networks, e.g., Fenton and Zweifach, 1981.) The remaining equations for the unknown RBC O_2 fluxes may be solved by standard numerical techniques.

The analysis to follow is performed in such a way that it allows for not only single erythrocytes but also clusters of RBCs as basic units of the model, even though in the formulation we shall refer to single erythrocytes only.

Assumptions

The simplifying assumptions underlying the present model are listed here and discussed in Appendix 2.

(*1*) As outlined above, tissue P_{O_2} distributions are built up from a particular solution satisfying the diffusion equation with consumption term plus a sum of solutions of the homogeneous equation, one for each RBC contained in the tissue. In the former term, a homogeneous O_2 consumption rate and homogeneous diffusion properties all over the domain of integration are assumed.

(*2*) For the latter terms of the solution to exist in the form of tractable analytical expressions, certain symmetry and homogeneity requirements have to be met: RBC and carrier-free layer must be bounded by surfaces that can be characterized by a constant value of one of the coordinates with respect to a suitable curvilinear coordinate system in space. Considering typical in vivo RBC shapes, modeling RBCs as prolate spheroids appeared to be most appropriate (see Fig. 1).

(*3*) Except for the central RBC of each of these particular solutions and its surrounding layer, the rest of the domain of integration is assumed homogeneous. Thus, variations in tissue diffusivity caused by the other RBCs and carrier-free layers are neglected.

(*4*) In matching the solution at the interface between tissue and carrier-free layer of each individual erythrocyte, the average value of the solution over the respective interface is required. In order to keep the problem numerically tractable, this average value is approximated by the value at the RBC center for each term of the solution other than the one appertaining to the carrier-free layer under consideration. For the latter one, a constant P_{O_2} at the RBC surface is assumed, resulting in a constant P_{O_2} at the interface also.

(*5*) The reaction between O_2 and the O_2 carrier in the tissue is assumed to reside in chemical equilibrium.

(*6*) The physiological situation described is assumed to be in steady state throughout.

Formulation

Let $\mathcal{T}$ denote a cuboid tissue region containing an O_2 carrier (myoglobin) at a concentration C_{Mb} (possibly $C_{Mb} = 0$) and a number of capillaries which hold (clusters of) erythrocytes E_i, $i = 1, \ldots m$ with volumes V_i, surface

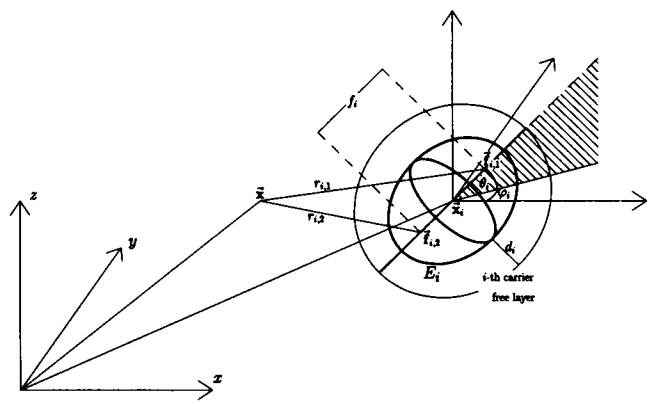

FIGURE 1 Geometry of single RBC E_i, positioned at $\vec{x}_i = (x_i, y_i, z_i)$ with foci $\vec{f}_{i,1}$ and $\vec{f}_{i,2}$. Interfocal distance is f_i, longitude and latitude of major semi axis are φ_i and θ_i, respectively. E_i is surrounded by a carrier-free layer which has the shape of a confocal prolate spheroid and the thickness of which (taken in the equatorial plane of the spheroid) is d_i. For an arbitrary vector $\vec{x}$, the distances $r_{i,1}$ and $t_{i,2}$ used in the construction of prolate spheroidal coordinates are shown.

areas σ_i, and hemoglobin concentrations C_{Hbi} (Fig. 2). Let $\mathcal{T}$ be positioned with one corner at the origin of a Cartesian coordinate system and let its length, width, and height be given by x_0, y_0, and z_0. E_i is positioned with its center at $\vec{x}_i = (x_i, y_i, z_i)$ and has the shape of a prolate spheroid with interfocal distance f_i, the direction of the major axis of which is given by its longitude φ_i and its latitude θ_i (Fig. 1). Let E_i be surrounded by a carrier-free layer which has the shape of a confocal prolate spheroid and the thickness of which (taken in the equatorial plane of the spheroid) is d_i.

Let $P(\vec{x})$ be the O_2 partial pressure distribution, let A be the O_2 consumption rate of the tissue, and let D_T, α_T, and D_L, α_L be the O_2 diffusion constants and the O_2 solubilities in the tissue or in the carrier-free layer, respectively. Let D_{Mb} denote the diffusivity of the O_2 carrier and $S(P) = P/(P + P_{50})$ its O_2 saturation, where P_{50} is its half-saturation P_{O_2}. Then the following system of partial differential equations has to be solved:

$$\begin{aligned} D_T\alpha_T\nabla^2 P + D_{Mb}C_{Mb}\nabla^2 S(P) &= A \quad \text{in the tissue,} \\ \nabla^2 P &= 0 \quad \text{in the carrier-free layer.} \end{aligned} \tag{1}$$

At the interface between tissue and carrier-free layer, P_{O_2} and the normal component of the total O_2 flux are to be continuous.

At a given point $\vec{x}$ on the boundary of the tissue region $\mathcal{T}$, neither P_{O_2} nor O_2 flux are known in advance. Rather, both of them depend on number, distances, and P_{O_2}s of the capillaries in a proximity of $\vec{x}$. The type of boundary conditions most commonly used (e.g., constant P_{O_2} or no flow boundary conditions) would disregard this fact and artificially force P_{O_2} or O_2 flux to assume a preset value. Therefore, we do not impose a local boundary condition and allow boundary P_{O_2} and O_2 fluxes to vary with the local distribution of RBCs and their O_2 saturation. On the other hand, if $\mathcal{T}$ is chosen large enough, the total net O_2 flow across the boundaries of $\mathcal{T}$ has to vanish. This is achieved by requiring

$$\sum_{i=1}^{m} \Phi_i = x_0 \cdot y_0 \cdot z_0 \cdot A, \tag{2}$$

where Φ_i is the O_2 flux out of erythrocyte E_i.

For each E_i the P_{O_2} averaged over the surface of E_i is to be equal to some $\bar{P}_{iE}$ which depends on the mean hemoglobin O_2 saturation $\mathcal{S}_i$ inside E_i and on the O_2 flux Φ_i out of E_i. Clark and Clark (1986) have determined $\bar{P}_{iE}$ to be as follows: Let the hemoglobin O_2 saturation $\mathcal{S}$ at an O_2 partial pressure P be approximated by Hill's equation

$$\mathcal{S} = \frac{(P/\mathcal{P}_{50})^n}{1 + (P/\mathcal{P}_{50})^n}, \tag{3}$$

where $\mathcal{P}_{50}$ is the half-saturation P_{O_2} of Hb and n is the Hill coefficient. Then

$$\bar{P}_{iE} = \mathcal{P}_{50} \sqrt[n]{\frac{\mathcal{S}_i}{1 - \mathcal{S}_i}} \left(1 - \frac{\Phi_i}{\sigma_i \sqrt{C_{Hbi} D_E \alpha_E K \mathcal{P}_{50} n \mathcal{S}_i}}\right), \tag{4}$$

where D_E and α_E are the diffusivity and the solubility of O_2 in the RBC and K is the rate constant of the O_2 dissociation from HbO_2.

The determination of the O_2 saturation $\mathcal{S}_i$ of a given RBC E_i requires knowledge of the "O_2 unloading history" of E_i within $\mathcal{T}$. To calculate this history explicitly for each E_i in $\mathcal{T}$ would be a tedious and computer time-consuming task. However, as in the present model, a steady-state situation, which is considered all of E_i's history, is contained within $\mathcal{T}$ already, in the form of E_i's successors. Therefore, we only need to interrelate the O_2 saturations $\mathcal{S}_i$ in adjacent erythrocytes. In order to do so, we need to know the time the RBC E_i took to travel from the nearest upstream RBC position to its present position, as this time determines the difference in O_2 content between the RBC

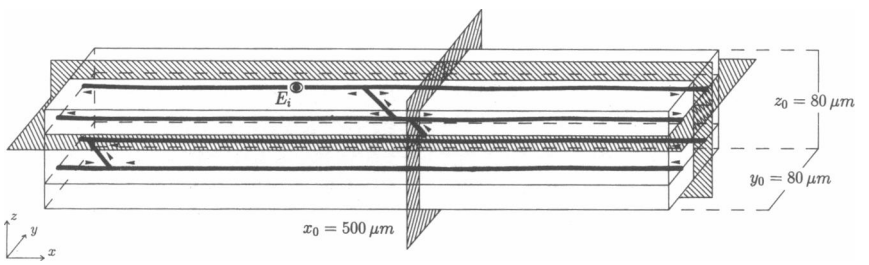

FIGURE 2 Geometry and dimensions of tissue region $\mathcal{T}$ modeled. A central muscle fiber is surrounded by four (rows of) capillaries (*bold lines*), two of them located in an upper level ($z = 60\ \mu m$) and two located in a lower level ($z = 20\ \mu m$). For reference, a sample RBC with its carrier-free layer (E_i) is outlined in one of the capillaries in the upper level. Capillary origins are staggered: The capillaries in the upper level are branches of a terminal arteriole which enters $\mathcal{T}$ from the front side at $x = 300\ \mu m$ and at an angle of 45°. The capillaries in the lower level drain into a collecting venule which leaves $\mathcal{T}$ at $y = 60\ \mu m$ through its left-hand side. Directions of flow are indicated by arrows. Hatched areas mark the section planes in which P_{O_2} distributions have been evaluated.

E_i and its successor. At this stage of model development we do not attempt to calculate these hemodynamic data from a network flow model. Rather, these data are described in terms detailed below and are input to the model from a data file. Note that the hemodynamic input data have to be generated in such a way that they are consistent with Kirchhoff's laws governing network flows.

Assume that the microvascular network in $\mathcal{T}$ contains diverging and converging bifurcations only (no multifurcations) and that each vascular segment holds at least one RBC. Then each RBC E_i in the network has either none (in the case of the first RBC in an inflow vessel) or one or two (in the case of a converging bifurcation) immediate successors among $\{E_i, i = 1, \ldots m\}$. We assume that E_i has one successor and deal with the case of a second successor in parentheses (. . .). Let the indices of the successors be k_i (and j_i). In the case of a converging bifurcation account has to be taken of the fact that $\mathcal{S}_i$ may vary depending on which branch of the bifurcation E_i originates from. This is done by choosing $\mathcal{S}_i$ to be the RBC flux weighted mean of the outflow saturations of both branches. To this end, let F_i be the fraction of the RBC flux in $\vec{x}_i$ that comes from location $\vec{x}_{k_i}$. Clearly, the RBC flux fraction coming from $\vec{x}_{j_i}$ is $(1 - F_i)$. If E_i is not positioned immediately downstream of a converging bifurcation then, of course, $F_i = 1$. Let the times a RBC takes to travel from $\vec{x}_{k_i}$ (or from $\vec{x}_{j_i}$) to $\vec{x}_i$ be denoted by t_i (or s_i).

Consider a RBC moving from $\vec{x}_{k_i}$ to $\vec{x}_i$ and suppose the oxygen flux at $\vec{x}_{k_i}$ is Φ_{k_i}, and at $\vec{x}_i$ is Φ_i. If we assume that the O_2 flux varies linearly with time during the transit from $\vec{x}_i$ to $\vec{x}_{k_i}$, then, for the transit time t_i, the flux out is $t_i/2(\Phi_i + \Phi_{k_i})$. [Accordingly, the O_2 flux during transit from $\vec{x}_{j_i}$ to $\vec{x}_i$ is $s_i/2(\Phi_i + \Phi_{j_i})$.] This allows us to calculate the mean O_2 content $\mathcal{S}_i C_{\mathrm{Hb}i} V_i$ of E_i from the O_2 contents of E_{k_i} (and of E_{j_i}):

$$\mathcal{S}_i C_{\mathrm{Hb}i} V_i = F_i \left[\mathcal{S}_{k_i} C_{\mathrm{Hb}k_i} V_{k_i} - \frac{t_i}{2} (\Phi_i + \Phi_{k_i}) \right] + (1 - F_i) \left[\mathcal{S}_{j_i} C_{\mathrm{Hb}j_i} V_{j_i} - \frac{s_i}{2} (\Phi_i + \Phi_{j_i}) \right]. \quad (5)$$

For RBCs without a successor inside $\mathcal{T}$, i.e., for RBCs at the arterial inflow, their O_2 saturation $\mathcal{S}_i$ has to be prescribed as a boundary condition. This whole scheme may be reversed: By adding RBC O_2 fluxes instead of subtracting them, successive RBC O_2 contents may be calculated originating from a prescribed venous outflow saturation. Formally, this case is covered by Eq. 5 if the t_i (and s_i) are assigned negative values. Eq. 5 furnishes the additional equations that are necessary to determine the mean O_2 saturation inside E_i and hence the boundary P_{O_2}, $\bar{P}_{iE}$.

Solution

The mathematical analysis of the diffusion problem proceeds along similar lines as outlined by Clark et al. (1989) and Hoofd et al. (1989). Following Hoofd et al. (1989) we define an effective O_2 partial pressure P^*:

$$P^* = P + \frac{D_{\mathrm{Mb}} C_{\mathrm{Mb}}}{D_T \alpha_T} S(P) = P + \frac{D_{\mathrm{Mb}} C_{\mathrm{Mb}}}{D_T \alpha_T} \frac{P}{P + P_{50}}. \quad (6)$$

Inversely, P may be obtained from P^* by

$$P = \frac{1}{2}\left(P^* - \frac{D_{\mathrm{Mb}} C_{\mathrm{Mb}}}{D_T \alpha_T} - P_{50}\right) + \frac{1}{2}\sqrt{\left(P^* - \frac{D_{\mathrm{Mb}} C_{\mathrm{Mb}}}{D_T \alpha_T} - P_{50}\right)^2 + 4P^* P_{50}}. \quad (7)$$

Substituting P^* in the tissue equation of Eq. 1 yields

$$\nabla^2 P^* = -\frac{A}{D_T \alpha_T}. \quad (8)$$

We are going to build up a solution of Eq. 8 according to

$$P^*(\vec{x}) = P_0^*(\vec{x}) + \sum_{i=1}^{m} P_i^*(\vec{x}), \quad (9)$$

where P_0^* is a solution of Eq. 8 with consumption and P_i^* solves the homogeneous Eq. 8.

Solution of Eq. 8 with consumption term

As can be seen by differentiating, a solution of Eq. 8 is given by

$$P_0^* = B_0 + \frac{A}{2D_T \alpha_T} \cdot \frac{1}{\frac{1}{x_0} + \frac{1}{y_0} + \frac{1}{z_0}} \cdot \left[\left(\frac{x}{x_0} - 1\right) x + \left(\frac{y}{y_0} - 1\right) y + \left(\frac{z}{z_0} - 1\right) z \right], \quad (10)$$

where B_0 is some constant still to be determined. The constants of integration are chosen in such a way that the O_2 flux densities across the boundary of $\mathcal{T}$ do not vary with position.

Solution of the homogeneous Eq. 8 for an erythrocyte E_i shaped as a prolate spheroid and surrounded by a confocal carrier-free layer

The analysis to be performed here is similar to the one presented by Clark and Clark (1985) who studied the P_{O_2} field of an isolated mitochondrion with homogeneous O_2 consumption. Basic definitions and equations are taken from or formed in analogy to Morse and Feshbach (1953), section 10.3.

In a first step, the Cartesian coordinates (x, y, z) are transformed to prolate spheroidal coordinates $(\xi_i, \eta_i, \omega_i)$ which are centered at $\vec{x}_i$ (see Appendix 1). In prolate

spheroidal coordinates, surfaces of confocal prolate spheroids are parameterized by $\xi_i = c$ for some constant c. In particular, the surfaces of the ith RBC and its carrier-free layer are characterized by $\xi_i = \xi_{iE}$ and by $\xi_i = \xi_{iL}$ with ξ_{iE} and ξ_{iL} as specified in Appendix 1.

The solutions of the Laplacian equation for a constant surface P_{O_2} at the erythrocyte (see assumption 4) are given by

$$P_i(\xi_i, \eta_i, \omega_i) = B_{iL} + C_{iL} \ln \frac{\xi_i + 1}{\xi_i - 1} \quad \text{in the carrier-free layer,}$$

$$P_i^*(\xi_i, \eta_i, \omega_i) = B_{iT} + C_{iT} \ln \frac{\xi_i + 1}{\xi_i - 1} \quad \text{in the tissue.} \tag{11}$$

As P_0^* still contains the undetermined constant B_0, one of the two B_{iL} or B_{iT}, say B_{iT}, may be chosen 0. At the RBC membrane ($\xi_i = \xi_{iE}$), P_{O_2} has to be equal to the red cell surface P_{O_2}, $\bar{P}_{iE}$, which is going to be substituted from Eq. 4. Thus,

$$B_{iL} = \bar{P}_{iE} - C_{iL} \ln \frac{\xi_{iE} + 1}{\xi_{iE} - 1}. \tag{12}$$

At the interface between carrier-free layer and tissue ($\xi_i = \xi_{iL}$), O_2 fluxes in the normal direction $\vec{n}$ and P_{O_2} have to be matched. According to assumption 3, the RBC E_i just "does not exist" in any of the terms of the solution in Eq. 8 other than the ith one. Therefore, fluxes in these terms are continuous at the interface by default and we need to deal with P_i and P_i^* only. We require

$$D_L \alpha_L \vec{n} \cdot \nabla P_i(\xi_{iL}, \eta_i, \omega_i) = D_T \alpha_T \vec{n} \cdot \nabla P_i^*(\xi_{iL}, \eta_i, \omega_i)$$

$$\rightarrow \quad D_L \alpha_L C_{iL} \frac{\partial}{\partial \xi_i} \ln \frac{\xi_i + 1}{\xi_i - 1}\bigg|_{\xi_i = \xi_{iL}} = D_T \alpha_T C_{iT} \frac{\partial}{\partial \xi_i} \ln \frac{\xi_i + 1}{\xi_i - 1}\bigg|_{\xi_i = \xi_{iL}}$$

$$\rightarrow \quad C_{iL} = \frac{D_T \alpha_T}{D_L \alpha_L} C_{iT}. \tag{13}$$

Finally, P_{O_2} has to be continuous at the interface between carrier-free layer and tissue. As P_{O_2} in the tissue depends on the effective P_{O_2}, P^*, in a nonlinear fashion (see Eq. 7), this requirement cannot be satisfied for the ith term of Eq. 9 alone and has to be dealt with when treating the boundary conditions. Altogether, Eqs. 11 may be rewritten:

$$P_i(\xi_i, \eta_i, \omega_i) = \bar{P}_{iE} + \frac{D_T \alpha_T}{D_L \alpha_L} C_{iT} \ln \frac{(\xi_i + 1)(\xi_{iE} - 1)}{(\xi_i - 1)(\xi_{iE} + 1)} \quad \text{in the carrier-free layer,}$$

$$P_i^*(\xi_i, \eta_i, \omega_i) = C_{iT} \ln \frac{\xi_i + 1}{\xi_i - 1} \quad \text{in the tissue.} \tag{14}$$

The total O_2 flux out of the erythrocyte E_i at the RBC surface is obtained by

$$\Phi_i = -D_L \alpha_L \iint_{\text{RBC surface } \sigma_i} \vec{n} \cdot \nabla P \Big|_{\xi_i = \xi_{iE}} d\sigma$$

$$= -D_L \alpha_L C_{iL} \int_0^{2\pi} \int_{-1}^{1} \frac{2}{f_i} \sqrt{\frac{\xi_{iE}^2 - 1}{\xi_{iE}^2 - \eta_i^2}} \cdot \frac{\partial}{\partial \xi_i} \ln \frac{\xi_i + 1}{\xi_i - 1}\bigg|_{\xi_i = \xi_{iE}} \cdot \frac{f_i^2}{4} \sqrt{(\xi_{iE}^2 - 1)(\xi_{iE}^2 - \eta_i^2)}\, d\eta_i\, d\omega_i$$

$$\Phi_i = D_T \alpha_T C_{iT} 4\pi f_i. \tag{15}$$

Boundary conditions

The remaining constants B_0 and C_{iT}, $i = 1, \ldots m$, are to be determined such that firstly Eq. 2 holds, i.e.:

$$\sum_{i=1}^{m} C_{iT} f_i = \frac{x_0 y_0 z_0 A}{4\pi D_T \alpha_T}. \tag{16}$$

Secondly, the O_2 saturations of adjacent RBCs need to be interrelated according to Eq. 5:

$$\mathcal{S}_i = \frac{F_i}{C_{\text{Hb}i} V_i} [\mathcal{S}_{k_i} C_{\text{Hb}k_i} V_{k_i} - D_T \alpha_T 2\pi t_i (C_{iT} f_i + C_{k_i T} f_{k_i})] \left\{ + \frac{1 - F_i}{C_{\text{Hb}_i} V_i} [S_{j_i} C_{\text{Hb}j_i} V_{j_i} - D_T \alpha_T 2\pi s_i (C_{iT} f_i + C_{j_i T} F_{j_i})] \right\}, \tag{17}$$

if E_i has one (or two) successors. The system of Eqs. 17 ($i = 1, \ldots m$) is explicit in $\mathcal{S}_i$, if the RBCs are numbered in such a way that successors always precede their predecessors (i.e., feed vessels to each vascular segment are numbered first) or vice versa if venous outflow saturations are specified.

Thirdly, for each RBC E_i, at the interface between carrier-free layer and tissue the mean P_{O_2}, $\bar{P}_{iL}$, needs to be calculated from $\mathcal{S}_i$ (Eq. 17) and from the intra-erythrocytic (Eq. 4) and the peri-erythrocytic (Eq. 14) P_{O_2} drops, and needs to be matched with mean P^* (Eqs. 9, 10, 14) via Eq. 6:

$$\bar{P}_{iL} = \sqrt[n]{\frac{\mathcal{S}_i}{1 - \mathcal{S}_i}} \left(\mathcal{P}_{50} - \frac{C_{iT} D_T \alpha_T 4\pi f_i \sqrt{\mathcal{P}_{50}}}{\sigma_i \sqrt{C_{\text{Hb}i} D_E \alpha_E K n \mathcal{S}_i}} \right) + C_{iT} \frac{D_T \alpha_T}{D_L \alpha_L} \ln \frac{(\xi_{iL} + 1)(\xi_{iE} - 1)}{(\xi_{iL} - 1)(\xi_{iE} + 1)} \tag{18}$$

$$\bar{P}_{iL} \left(1 + \frac{D_{\text{Mb}} C_{\text{Mb}}}{D_T \alpha_T} \frac{1}{\bar{P}_{iL} + P_{50}} \right) = B_0 + \frac{A}{2 D_T \alpha_T} = \cdot \frac{1}{\frac{1}{x_0} + \frac{1}{y_0} + \frac{1}{z_0}} \cdot \left[\left(\frac{x_i}{x_0} - 1 \right) x_i + \left(\frac{y_i}{y_0} - 1 \right) y_i + \left(\frac{z_i}{z_0} - 1 \right) z_i \right] + C_{iT} \ln \frac{\xi_{iL} + 1}{\xi_{iL} - 1} + \sum_{\substack{l=1 \\ l \neq i}}^{m} C_{lT} \ln \frac{\xi_l(\vec{x}_i) + 1}{\xi_l(\vec{x}_i) - 1}, \tag{19}$$

where ξ_{iL} is from Eq. 25 and $\xi_l(\vec{x}_i)$ is calculated according to Eqs. 22 and 23 (see Appendix 1). Eqs. 16–19 form a system of $m + 1$ nonlinear equations in the unknowns B_0, C_{iT}, $i = 1, \ldots m$, which has to be solved numerically.

APPLICATION

The model has been applied to a situation in heavily working skeletal muscle shown in Fig. 2. The size of the tissue region modeled is 500 × 80 × 80 μm. A central muscle fiber of an equivalent diameter of 45 μm is surrounded by four (rows of) capillaries, two of them located in an upper level and two located in a lower level. Capillary origins are staggered: The capillaries in the upper level are branches of a terminal arteriole which enters $\mathcal{T}$ from the front side at $x = 300$ μm and at an angle of 45°. The capillaries in the lower level drain into a collecting venule which leaves $\mathcal{T}$ at $y = 60$ μm through its left-hand side.

The data used in the evaluation are compiled in Table 1. All of them are typical of dog gracilis muscle working at a twitch frequency of 8 Hz. Number, positions, and interrelations of RBCs are chosen in agreement with measurements of capillary density, blood flows (Honig and Odoroff, 1981), and intracapillary RBC spacing (Honig, personal communication) in dog gracilis. This procedure resulted in 243 RBCs inside $\mathcal{T}$ and, consequently, in 244 equations in the system to be solved. RBC inflow saturation in the terminal arterioles is taken to be 90% from cryophotometric measurements in terminal arterioles (Honig, C. R., K. Groebe, and T. E. J. Gayeski, manuscript submitted for publication), outflow saturation in collecting venules is taken to be 42% (Honig and Odoroff, 1981). The interfocal distance f_i is determined such that the resulting RBC shape is close to the one that can be observed on in vivo microphotographs of the capillary bed (see, e.g., Skalak and Branemark, 1969). The choice of the blood parameters has been discussed by Clark et al. (1985). For dimension and diffusivity of the carrier-free layers, no experimental data are available. Therefore, their thickness is estimated from electron-

TABLE 1 Parameter values employed in the numerical evaluation

A = O_2 consumption rate of the tissue	$= 16 \frac{\text{ml } O_2}{100\text{g} \cdot \text{min}}$	(Gayeski et al., 1987)
α_E = O_2 solubility in the RBC	$= 1.56 \cdot 10^{-9} \frac{\text{mol}}{\text{cm}^3 \cdot \text{mm Hg}}$	(Clark et al., 1985)
α_L = O_2 solubility in the carrier-free layer	$= 9.4 \cdot 10^{-10} \frac{\text{mol}}{\text{cm}^3 \cdot \text{mm Hg}}$	(Zander, 1975)
α_T = O_2 solubility in the tissue	$= 9.4 \cdot 10^{-10} \frac{\text{mol}}{\text{cm}^3 \cdot \text{mm Hg}}$	(Zander, 1975)
C_{Hb} = total Hb monomer concentration in the RBC	$= 2.03 \cdot 10^{-2}$ mol/l	(Clark et al., 1985)
C_{Mb} = Total Mb concentration in the muscle fiber	$= 5.4 \cdot 10^{-4}$ mol/l	(Wittenberg, 1970)
D_E = O_2 diffusion coefficient in the RBC	$= 9.5 \cdot 10^{-6}$ cm^2/s	(Clark et al., 1985)
D_L = O_2 diffusion coefficient in the carrier-free layer	$= 1.65 \cdot 10^{-5}$ cm^2/s	(Vaupel, 1976)
D_{Mb} = Mb diffusion coefficient in 18% protein solution	$= 8.0 \cdot 10^{-7}$ cm^2/s	(Riveros-Moreno and Wittenberg, 1972)
D_T = O_2 diffusion coefficient in muscle	$= 1.16 \cdot 10^{-5}$ cm^2/s	(Homer et al., 1984)
d_l = thickness of carrier-free layer in the equatorial plane	$= 1.55$ μm	(Brodal et al., 1977)
f_i = interfocal distance of RBC	$= 3.8$ μm	
K = dissociation rate constant of HbO_2	$= 44$ s^{-1}	(Clark et al., 1985)
n = Hill coefficient of Hb	$= 2.65$	(Clark et al., 1985)
$\mathcal{P}_{50}$ = half saturation P_{O_2} of Hb	$= 26.4$ mm Hg	(Clark et al., 1985)
P_{50} = half saturation P_{O_2} of Mb	$= 5.3$ mm Hg	(Gayeski and Honig, 1986)
V_i = RBC volume	$= 66$ fl	(Altman and Dittmer, 1972)
capillary density	$= 625$ mm^{-2}	(Honig and Odoroff, 1981)
blood flow rate	$= 130 \frac{\text{ml}}{100\text{ g} \cdot \text{min}}$	(Honig and Odoroff, 1981)
average inter-erythrocytic gap length	$= 3$ μm	
resulting RBC velocity	$= 2$ mm/s	

All data refer to 37° C. Capillary density and hemodynamic data do not enter the model equations directly but via an appropriate choice of RBC positions and transit times t_l and s_l (cf. Eq. 5).

microscopic cross sections through muscle capillaries (see, e.g., Brodal et al., 1977). An estimated average water content of 85% is used to obtain O_2 solubility and O_2 diffusion coefficient from the respective relationships established by Zander (1975) and Vaupel (1976).

Calculations were performed on the Honeywell Bull Multics system (Johannes Gutenberg-Universität, Mainz, West Germany). For the solution of the resulting nonlinear system of equations, a modified Powell hybrid method (routine C05PCF of The NAG Fortran Library, Mark 12 by The Numerical Algorithms Group, Oxford, UK) was used. In spite of its magnitude, the nonlinear system of equations is very well conditioned. Once the QR factorization of its Jacobian was calculated, the algorithm needed only nine function calls to converge to a precision of 10^{-7}.

Figs. 3–5 show P_{O_2} distributions calculated in the three planes marked in Fig. 2. Resulting P_{O_2} gradients are steepest in the perivascular region, whereas the profiles are essentially flat in the rest of the tissue. In order to study this pattern more closely, Fig. 6 shows typical one-dimensional P_{O_2} profiles calculated from the model in the equatorial plane of some selected RBCs. Inside the RBCs, the model does not furnish P_{O_2} profiles. The data points inside the RBCs therefore give the mean intra-erythrocytic P_{O_2} and the P_{O_2} at the RBC surface, respectively. In all of the profiles, P_{O_2} drops very steeply across the carrier-free layer and across the first few micrometers of the tissue. Further into the muscle fiber, gradients become shallower and the P_{O_2} levels are virtually independent of the surface P_{O_2} of the RBC considered.

DISCUSSION

The model suggested describes steady state P_{O_2} distributions in myoglobin containing tissue for arbitrary arrangements of red blood cells which are surrounded by carrier-free layers of arbitrary thicknesses. The basic units that build up a P_{O_2} distribution are the diffusion

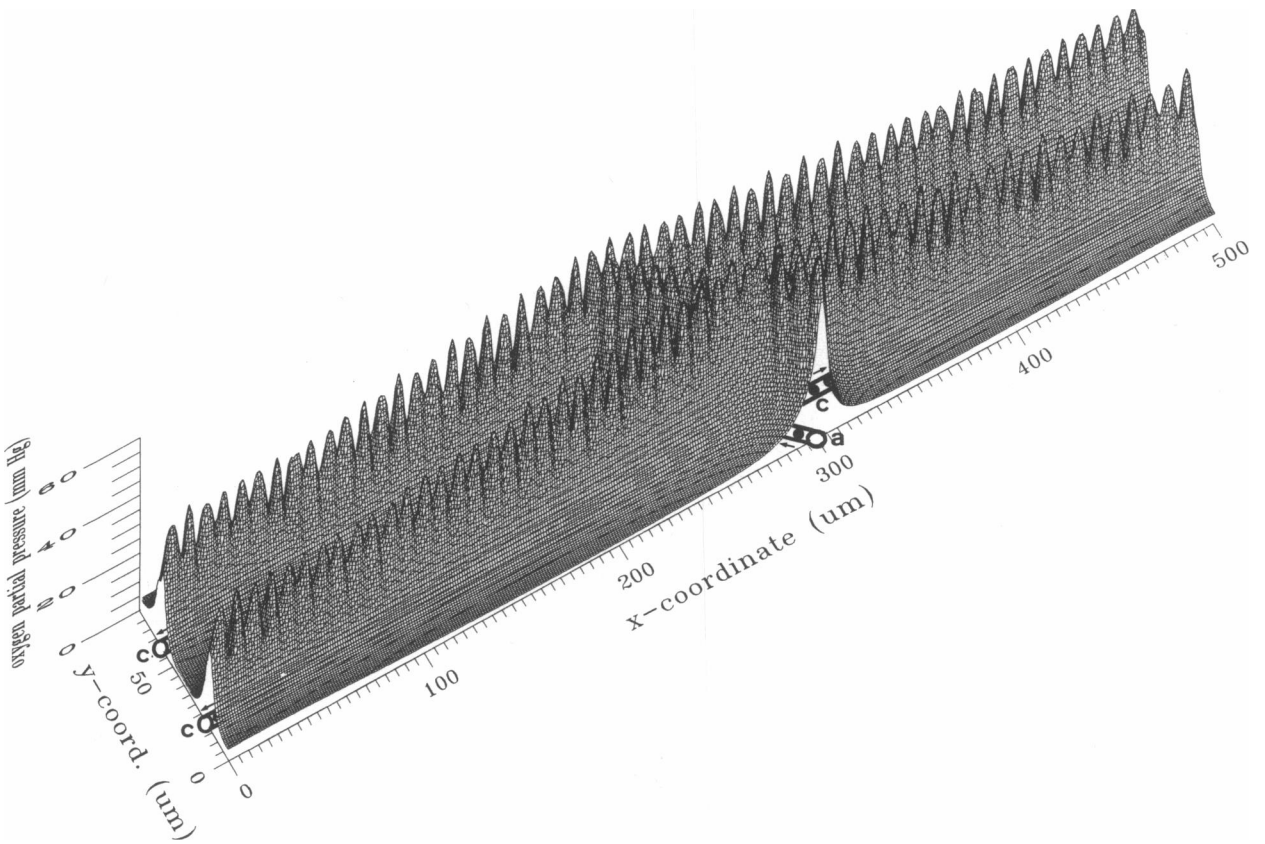

FIGURE 3 P_{O_2} distribution in a horizontal section through the upper capillary level of the model (cf. Fig. 2). The outflow portions of two capillaries (*c*) and the inflow portion of the terminal arteriole (*a*) and of one capillary (*c*) with their carrier-free layers (*bold lines*) and with RBCs contained in their lumina are traced at the left and in the center of the base plane, respectively. Arrows indicate directions of flow. Even though the length of $\mathcal{T}$ is 500 μm, the P_{O_2} drops surrounding each individual RBC are still resolved.

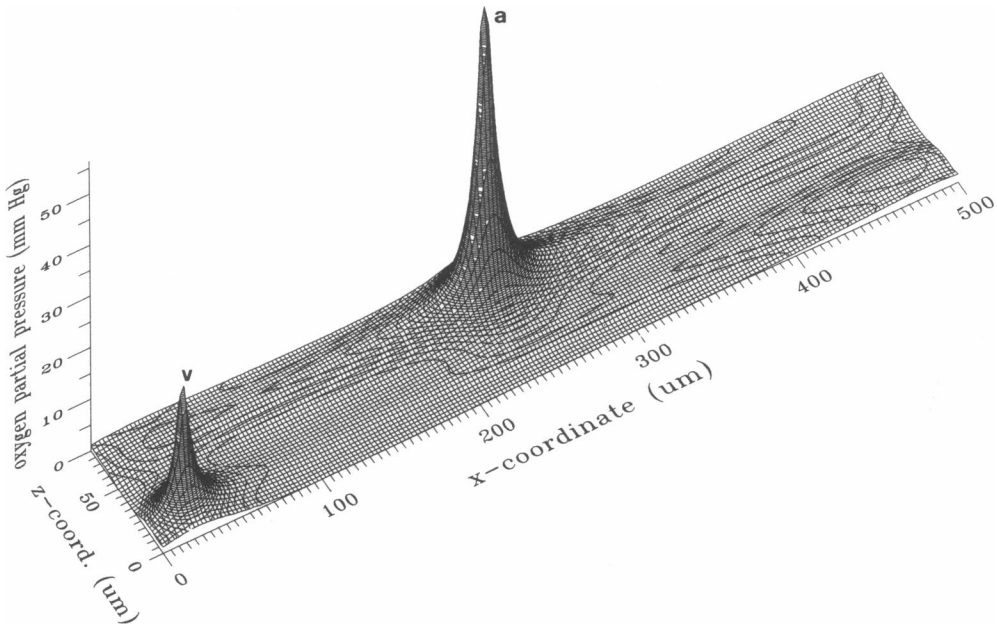

FIGURE 4 P_{O_2} distribution in a vertical plane through the fiber axis (cf. Fig. 2). Except for the terminal arteriole (*a*) in the center and the collecting venule (*v*) at the left, this section does not contain any microvessels and exhibits a low and uniform P_{O_2} profile with shallow P_{O_2} elevations in both of the capillary levels ($z = 20$ μm and $z = 60$ μm).

fields of prolate spheroids with concentric carrier-free layers. By considering variable volumes, carrier-free layer thicknesses, etc. in these basic units, the model allows not only for single erythrocytes but also for erythrocyte clusters or whole RBC-filled vessel segments (in which the plasma portion of the blood may be roughly considered by an appropriately decreased hemoglobin concentration and an adjusted effective O_2 diffusion coefficient) as O_2 sources as well. It is of interest that for the data set used in the application of the model the resulting P_{O_2} distribution remains virtually unchanged if the interfocal distance of the prolate spheroids representing the RBCs is decreased. This observation suggests that in the present application analysis could be simplified by assuming spherical symmetry for the diffusion fields of individual erythrocytes. The errors in the P_{O_2} profiles resulting from the model primarily depend on how well a given vascular network and the RBCs contained in it can be approximated by a set of hemoglobin-filled prolate spheroids with confocal carrier-free layers. Simultaneously with the computation of the tissue P_{O_2} distribution, estimates of the O_2 saturation of "downstream" prolate spheroids are obtained from the O_2 fluxes out of "upstream" prolate spheroids or vice versa. Consequently, if RBC fluxes in the network and inflow or outflow O_2 saturations are known, an O_2 distribution in all of the tissue considered, including RBC O_2 contents, results. Simplifying assumptions that were made in model formulation are discussed in Appendix 2.

Other models of combined convective and diffusive O_2 transport to tissue

Many of the models developed to calculate tissue P_{O_2} distributions assume a fixed P_{O_2} at the capillary–tissue interface and do not include RBC O_2 unloading. The models of this type that are relevant to the present work are discussed in the next section. In the past there have also been a number of approaches to modeling combined convective and diffusive O_2 transport to tissue. Recent reviews have been given by Grunewald and Sowa (1977), Fletcher (1978), Popel (1980), and Bruley (1980).

Roughly, these models may be divided into two classes: Firstly, the ones that retain the basic assumption of the classical Krogh equation and treat a capillary and its supply region as an independent unit. The relatively simple geometry allows them to consider additional features like Mb-facilitated O_2 transport, including its reaction kinetics and non–steady state O_2 supply. However, they cannot be used to answer the kind of questions raised in the introduction. Furthermore, the Krogh-type models published so far do not consider the particulate nature of

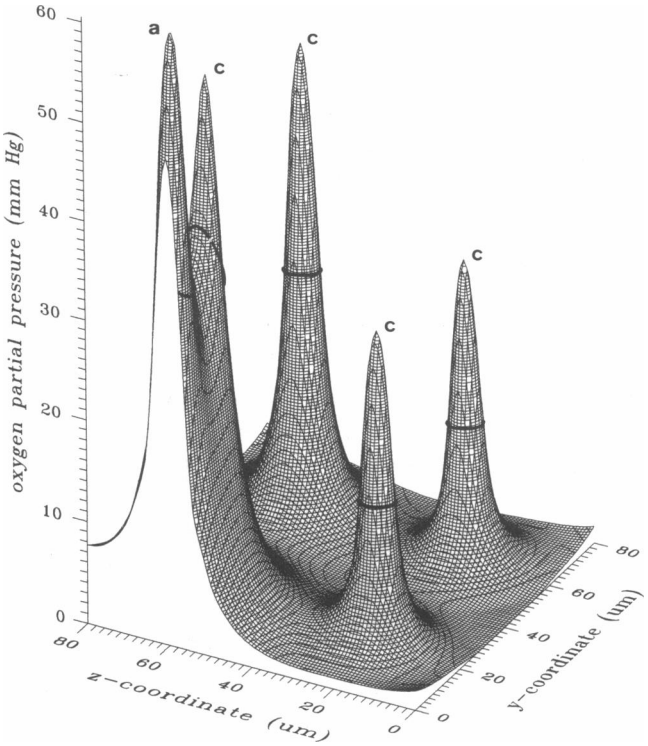

FIGURE 5 P_{O_2} distribution in a cross section through $\mathcal{T}$ at $x = 300$ μm (cf. Fig. 2). The entry of the terminal arteriole (*a*) and the two arterial capillary portions (*c*) of the upper capillary level are located to the left, whereas the two venous capillaries (*c*) of the lower level may be identified at the right. The boundaries between myocytes and carrier-free layers are delineated by bold lines.

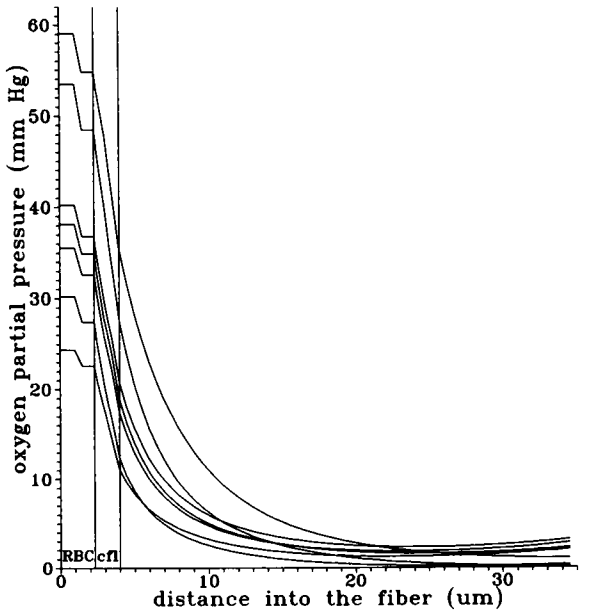

FIGURE 6 One-dimensional P_{O_2} profiles in the equatorial planes of some selected RBCs which cover the range of O_2 saturations and spatial variability found from the model. The locations of RBC and carrier-free layer are marked by "RBC" and "cfl," respectively. The data points inside the RBCs give the mean intra-erythrocytic P_{O_2} and the P_{O_2} at the RBC surface, respectively.

blood (cf. Federspiel and Popel, 1986) and a carrier-free layer surrounding the erythrocytes, both of which turn out to represent essential constituents of the P_{O_2} distributions found in heavily working skeletal muscle (see below).

The second class comprises the models that describe more complex capillary geometries and flow patterns and that allow one to study interactions between supply regions of adjacent capillaries and the effects of perfusion heterogeneities. Except for the stochastic approaches (see Bruley, 1980), each of the models of the second class is confined to a very special capillary geometry which is predetermined by the method applied for the solution of the resulting system of differential equations. In addition, the models of this class published so far do not consider carrier-facilitated O_2 diffusion, intracapillary P_{O_2} drops (cf. Hellums, 1977), or the particulate nature of blood (cf. Federspiel and Popel, 1986). On the other hand, the stochastic models which allow one to consider all of these and more features and which probably offer the most versatile approach there is, are impractical to date because of their immense requirements in computing time.

The present model appears to be a fair compromise between a variety of features that possibly could be included in a tissue O_2 supply model and cost efficiency in terms of computing time required for its application. Most importantly, it offers full flexibility with respect to vascular geometries and blood flows and to intravascular RBC distributions, and considers carrier-facilitated diffusion in RBCs and tissue, and a carrier-free layer in between.

O_2 transport in skeletal muscle

Figs. 3–5 give a general impression of the three-dimensional P_{O_2} distribution in heavily working skeletal muscle. Fig. 3 displays the P_{O_2} in a horizontal section through the upper capillary level of the model (cf. Fig. 2), viewed along the fiber axis and in an angle of 45°. Even though the length of $\mathcal{T}$ is 500 μm which is about half the length of capillaries in dog gracilis (Honig, personal communication), the P_{O_2} drops surrounding each individual RBC are still resolved. Note, however, that the model assumes steady state, even on a microscale (see above). As was shown by Groebe and Thews (1989), in real tissue

oscillations of capillary P_{O_2} along the capillary axis tend to be less pronounced. In Fig. 4, the P_{O_2} distribution in a vertical plane through the fiber axis is presented. Except for the terminal arteriole in the center and the collecting venule at the left, this section does not contain any vessels and exhibits a low and uniform P_{O_2} profile with shallow P_{O_2} elevations in both of the capillary levels. Fig. 5 depicts the P_{O_2} in a cross section through $\mathcal{T}$ at $x = 300$ μm. The entry of the terminal arteriole and the two arterial capillary portions of the upper capillary level are located to the left, whereas the two venous capillaries of the lower level may be identified at the right. More quantitative information may be drawn from Fig. 6, showing one-dimensional profiles in the equatorial planes of some selected RBCs which cover the range of O_2 saturations and spatial variability found from the model.

Steep perivascular gradients and shallow ones inside of the muscle fiber remote from capillaries agree very well with experimental findings by Gayeski and Honig (1986). To understand this characteristic P_{O_2} distribution, we recall that a P_{O_2} gradient is the ratio of the O_2 flux density over the effective O_2 conductivity. Therefore, P_{O_2} gradients are steepest where O_2 flux densities are highest: In our example, all of the O_2 consumed in a tissue region of 3,200 pl originates from 243 RBCs with an aggregate volume of only 16 pl and an aggregate surface area of 19,367 μm^2, resulting in a mean flux density of 0.22 fmol/(s μm^2) and a P_{O_2} gradient of 13.9 mmHg/μm at the RBC surface. Remote from the capillaries, O_2 flux densities become smaller and hence P_{O_2} gradients shallower (see Fig. 6).

Secondly, O_2 is transported across the carrier-free layer (which surrounds each RBC and which consists of a plasma sleeve, the capillary endothelium, and the interstitial space) solely by plain diffusion. This implies that the lowest effective O_2 conductivity along the O_2 diffusion path is found at the sites with the largest O_2 flux densities, which also contributes to the characteristic P_{O_2} distributions.

Thirdly, Mb facilitation of O_2 transport inside the muscle fiber is a decreasing function of P_{O_2}: The facilitated O_2 flux, $D_{Mb}C_{Mb}\nabla S(P)$, is maximal at $P = 0$ mmHg and decreases as P_{O_2} increases. At high P_{O_2} values $S(P) = P/(P + P_{50})$ is practically constant and facilitation is absent. As a consequence, there is almost vanishing resistance to O_2 diffusion and hence only negligible P_{O_2} gradients far into the fiber where P_{O_2}s are very low. In contrast, effective O_2 conductivity next to the interface between carrier-free layer and fiber depends on RBC surface P_{O_2}. In our examples, it amounts to 1.2 or 2.4 times the conductivity in the layer next to RBCs at arterial or venous O_2 saturation, respectively, whereas this factor increases to 6.0 in the fiber center. Consequently, there is more diffusion resistance next to RBCs with high surface P_{O_2}s as compared with RBCs with lower surface P_{O_2}s. Thus, there exists a P_{O_2} dependent "layer deficient of functional carrier," extending into the myoglobin containing tissue near RBCs with high surface P_{O_2}s. This has two important consequences: It results in a homogenization of RBC O_2 fluxes as compared with the heterogeneity of P_{O_2} drops between RBC surface and tissue. Secondly, the layer deficient of functional carrier serves as a reserve of O_2 conductance which is automatically recruited as capillary P_{O_2} falls and which promotes O_2 extraction and $\dot{V}_{O_2}$ in heavy exercise.

Both small variations in RBC O_2 fluxes and P_{O_2}-dependent layer deficient of functional carrier are illustrated in Fig. 6: P_{O_2} drops across the carrier-free layer (cfl) which are in proportion to O_2 flux densities are similar for all RBCs shown even though RBC surface P_{O_2} varies between 59 and 24 mmHg. On the other hand, P_{O_2} gradients are almost identical on either side of the interface for RBCs with high surface P_{O_2}s, suggesting the persistence of the layer deficient of functional carrier into the fiber, whereas there is a pronounced break in the profiles for RBCs with low surface P_{O_2}s. Corresponding P_{O_2} drops across the first 10 μm into the fiber vary between 29.5 mmHg and 9 mmHg. 10 μm or more into the fiber, P_{O_2} is nearly constant all over the tissue region modeled (cf. Gayeski and Honig, 1986).

Homogeneous O_2 fluxes along the capillary lead to a situation in which O_2 diffusion along the fiber axis is unimportant and hence longitudinal P_{O_2} gradients are small. This corresponds well with experimental findings by Gayeski and Honig (1988) and is also reflected in the results of the present model: Longitudinal P_{O_2} gradients in the capillary and at the interface are ~0.1 mmHg/μm near the arterial capillary ending and ~0.02 mmHg/μm near the venous capillary ending, whereas they are typically $<10^{-3}$ mmHg/μm in the fiber axis.

P_{O_2} distributions in myoglobin containing muscle tissue have been calculated by a number of researchers (Murray, 1974; Fletcher, 1980; Federspiel, 1986; Groebe and Thews, 1986; Hoofd et al., 1989; Clark et al., 1989). In most studies, however, either O_2 consumption rate and/or capillary geometry considered were grossly different from the ones in the present study, or the O_2 was allowed to enter the domain of integration across all or a large portion of its surface without an interposed carrier-free layer. Consequently, the characteristic shapes of the resulting P_{O_2} profiles are very different from the ones found in the present study.

Federspiel (1986) has modeled two-dimensional P_{O_2} profiles in a maximally consuming fiber. Surface P_{O_2} was set arbitrarily well below capillary P_{O_2} to take account of a large ΔP_{O_2} across the carrier-free region which was not included in the model. His resulting profiles exhibit shapes similar to the ones in our tissue region, even

though his layer deficient of functional carrier (i.e., his layer of well-saturated myoglobin) is not as pronounced as in the present study. This is due to the larger surface area of his O_2 sources which results in smaller O_2 flux densities and P_{o_2} gradients near the boundary.

In the three-dimensional model by Groebe and Thews (1986), a cylindrical fiber is surrounded by a carrier-free layer, on the surface of which an arbitrary P_{o_2} distribution may be prescribed. A three-dimensional approach was chosen because in two-dimensional models it is implicitly understood that the capillary holds a RBC column without interposed plasma gaps. At gap lengths of one-half RBC length, two-dimensional models overestimate the effective O_2 exchange area by roughly 50% which leads to P_{o_2} gradients near the RBC which are by one-third too small (cf. Hellums, 1977). This was the first attempt to include both carrier-free layers surrounding the erythrocytes and the myocyte in one and the same mathematical model. The results confirmed the experimentally found distribution of skeletal muscle P_{o_2} gradients (Gayeski and Honig, 1986). The major shortcoming of this model is, however, that the P_{o_2} dependence of Mb facilitation of O_2 transport was not considered, so the influence of a layer deficient of functional carrier could not be demonstrated. Nevertheless these former results are in qualitative agreement with the ones from the present model.

In conclusion, the model presented in this paper combines a number of features (see listing in the Introduction) of which only one or the other were present in former models of combined convective and diffusive O_2 transport to tissue. Some of its features have been studied so far in isolated partial models only (e.g., intra-erythrocytic P_{o_2} drops in RBC models such as Clark et al. [1985] or effects of the particulate nature of blood in capillary models such as Federspiel and Popel [1986] and Groebe and Thews [1989]). Other than the stochastic models (Bruley, 1980) which also allow for all of these features, the present model remains numerically tractable even in large tissue volumes.

The present application of the model has reconfirmed and extended previous experimental and theoretical findings on P_{o_2} distributions in heavily working skeletal muscle. The reasons for the characteristic P_{o_2} profiles found—steep perivascular gradients and low, homogeneous P_{o_2} values in the rest of the fiber—are threefold: High O_2 flux densities next to capillaries, low diffusivity in the carrier-free layer (as compared with the fiber interior), and low effective O_2 conductivity in a layer deficient of functional carrier extending from the carrier-free layer into the muscle fiber. In order to explain the typical shape of the P_{o_2} profiles, it is not necessary to hypothesize a capillary O_2 diffusion barrier.

The dimensions of the layer deficient of functional carrier depend on capillary P_{o_2} and on O_2 consumption rate in the tissue. As capillary P_{o_2} goes down and as O_2 consumption rate goes up its thickness decreases. The layer deficient of functional carrier therefore represents a reserve of O_2 conductance which is automatically recruited in exercise. This helps to explain how $\dot{V}_{o_2}$ can be increased up to 100-fold and O_2 extraction can be doubled in rest-work transition, despite a decrease in RBC transit times to one-seventh and an increase in effective capillary surface area by no more than 65% (data from Honig and Odoroff [1981] and Honig, personal communication).

APPENDIX 1

Coordinate transformations

Cartesian coordinates (x, y, z) are transformed to prolate spheroidal coordinates $(\xi_i, \eta_i, \omega_i)$ which are centered at $\vec{x}_i$. The foci of the erythrocyte E_i [positioned at $\vec{x}_i = (x_i, y_i, z_i)$, interfocal distance f_i, longitude and latitude of major semiaxis φ_i and θ_i, respectively; cf. Fig. 1] are

$$\vec{f}_{i,1} = \left(x_i + \frac{f_i}{2}\cos\varphi_i\cos\theta_i,\ y_i + \frac{f_i}{2}\sin\varphi_i\cos\theta_i,\ z_i + \frac{f_i}{2}\sin\theta_i\right),$$

$$\vec{f}_{i,2} = \left(x_i - \frac{f_i}{2}\cos\varphi_i\cos\theta_i,\ y_i - \frac{f_i}{2}\sin\varphi_i\cos\theta_i,\ z_i - \frac{f_i}{2}\sin\theta_i\right). \tag{20}$$

Two orthogonal vectors of length unity in the equatorial plane of E_i are:

$$\vec{e}_{i,1} = (-\sin\varphi_i, \cos\varphi_i, 0),$$
$$\vec{e}_{i,2} = (\cos\varphi_i\sin\theta_i, \sin\varphi_i\sin\theta_i, -\cos\theta_i). \tag{21}$$

Let $\vec{x} = (x, y, z)$ be the vector to be transformed and let $r_{i,1}$ and $r_{i,2}$ denote the distances between $\vec{x}$ and $\vec{f}_{i,1}$ or $\vec{f}_{i,2}$, respectively:

$$r_{i,1} = \sqrt{\left(x - x_i - \frac{f_i}{2}\cos\varphi_i\sin\theta_i\right)^2 + \left(y - y_i - \frac{f_i}{2}\sin\varphi_i\sin\theta_i\right)^2 + \left(z - z_i - \frac{f_i}{2}\cos\theta_i\right)^2},$$

$$r_{i,2} = \sqrt{\left(x - x_i + \frac{f_i}{2}\cos\varphi_i\sin\theta_i\right)^2 + \left(y - y_i + \frac{f_i}{2}\sin\varphi_i\sin\theta_i\right)^2 + \left(z - z_i + \frac{f_i}{2}\cos\theta_i\right)^2}. \tag{22}$$

Then prolate spheroidal coordinates are defined by

$$\xi_i = \frac{r_{i,1} + r_{i,2}}{f_i};\quad \eta_i = \frac{r_{i,1} - r_{i,2}}{f_i};\quad \omega_i = \arctan\frac{\vec{e}_{i,1}\cdot(\vec{x} - \vec{x}_i)}{\vec{e}_{i,2}\cdot(\vec{x} - \vec{x}_i)}. \tag{23}$$

The surfaces parameterized by ξ_i = const are confocal prolate spheroids with foci $\vec{f}_{i,1}$ and $\vec{f}_{i,2}$. The surfaces of the RBC and the carrier-free layer are characterized by $\xi_i = \xi_{iE}$,

$$\xi_{iE} = \frac{1}{f_i}\left(\sqrt{9\frac{V_i^2}{\pi^2} - \frac{f_i^6}{27}} + 3\frac{V_i}{\pi}\right)^{1/3} + \frac{f_i}{3}\left(\sqrt{9\frac{V_i^2}{\pi^2} - \frac{f_i^6}{27}} + 3\frac{V_i}{\pi}\right)^{-1/3}, \quad (24)$$

where V_i is the volume of RCB E_i and by $\xi_i = \xi_{iL}$

$$\xi_{iL} = \sqrt{\left(\sqrt{\xi_{iE}^2 - 1} + \frac{2d_i}{f_i}\right)^2 + 1}, \quad (25)$$

where d_i is the thickness of the carrier-free layer in the equatorial plane, respectively.

APPENDIX 2

Simplifying assumptions and possible extensions

The boundary conditions

As biological tissues do not exhibit regular geometries, on the edge of $\mathcal{T}$ neither local boundary P_{O_2}'s nor local boundary O_2 fluxes are known in advance. The choice of a constant P_{O_2} or a no flow boundary condition would be a very arbitrary one as it would force P_{O_2} or O_2 flux to assume values that can be predicted to be incorrect at least in many sites (e.g., if the arterial portion of a capillary is located next to the boundary, O_2 flux there is directed outward and boundary P_{O_2} is certainly higher than average). Thus, what one would like to do is calculate the real boundary P_{O_2}'s and O_2 fluxes from the model. But then the vascular geometry, blood flows, etc. from outside $\mathcal{T}$ would have to be known and the boundary would not be a boundary any more but an interface. Therefore, the best one can do is to use all the information one has from inside $\mathcal{T}$ to approximate the true boundary P_{O_2} and flux, and to assume that $\mathcal{T}$ is surrounded by a homogeneous "average" tissue in which the O_2 consumed and the O_2 unloaded from RBCs balance. This corresponds to a boundary value problem in which $\mathcal{T}$ is embedded in an infinite nonconsuming medium exhibiting the same diffusion properties as $\mathcal{T}$, with a finite and constant boundary P_{O_2} at infinity and with the average O_2 flux across the boundary of $\mathcal{T}$ vanishing. We proceed along these lines by constructing the P_{O_2} distribution as a sum of (infinite) particular solutions for individual RBCs and by requiring that overall RBC O_2 flux and O_2 consumption are balanced.

Basic unit geometry

Prolate spheroids and the P_{O_2} field associated with them have been chosen as the basic unit of the present model. From the assumptions section it becomes clear, however, that other basic units based on different curvilinear coordinate systems in space (e.g., spheres and polar coordinates) could have been chosen as well. Different basic unit geometries may be mixed in one and the same model to achieve more geometrical flexibility.

Assumption of steady state

Steady state conditions are, on a macro scale, a good approximation to many physiological situations of interest. On the scale of an individual red cell, however, there is no steady state! Moving RBCs give rise to oscillations in pericapillary P_{O_2} and O_2 fluxes (cf. Federspiel and Popel, 1986) which are damped at increasing RBC velocities if O_2 storage in the pericapillary tissue is considered (Groebe and Thews, 1989). Therefore, the results of the present model (and any steady state model resolving the particulate nature of blood) are no more than instantaneous snapshots of a continuously changing tissue P_{O_2} distribution in which (depending on RBC velocity) longitudinal variability of P_{O_2} in and next to capillaries is somewhat smaller than predicted. As the present tissue O_2 supply model does not primarily aim at highly spatially resolved capillary P_{O_2} distributions (these may be obtained from capillary O_2 unloading models, e.g., Groebe and Thews [1986, 1989]) this kind of deviation from the real situation appears to be acceptable. However, more severe errors may be introduced by an increase in RBC O_2 mass transfer coefficient induced by RBC movement as it affects the overall P_{O_2} drop between RBC membrane and tissue. This becomes particularly important at high RBC velocities and wide RBC spacings. In the above application, RBC movement would increase the effective diffusivity inside the carrier-free layer by no more than 1–2% (Groebe and Thews, 1989) and thus would not significantly change the resulting P_{O_2} profiles. For large RBC spacings and high RBC velocities any steady state model will significantly overestimate P_{O_2} drops between RBCs and tissue unless the effects of RBC movement are accounted for by an according increase in effective carrier-free layer O_2 conductance.

Homogeneous diffusion fields in P_i^*; average P_i^* at interfaces

In the P_{O_2} field of each erythrocyte all other erythrocytes and carrier-free layers (cfl) are assumed "not to exist," i.e., in the basic solutions P_i^*, $i = 0, \ldots m$, the differences between tissue diffusivity and the diffusivities inside RBCs E_j ($j \neq i$) and inside the carrier-free layers associated with them, are neglected. As a consequence, in the model O_2 from any RBC is allowed to diffuse through adjacent RBCs and cfls even though their higher P_{O_2} would not allow that. Remote from E_i ($i \neq 0$; for $i = 0$ this is true in all of the domain of integration), the error introduced by this simplification is not severe as major gradients in P_i^* ($i \neq 0$) are found next to E_i only and gradients far from E_i are very shallow anyway. For the same reason, in this situation $P_i^*(\vec{x}_j)$ ($j \neq i$) is a good approximation to the average P_i^* over the interface between jth carrier-free layer and the tissue. However, this simplification may cause troubles in the immediate vicinity of E_i where steep P_{O_2} gradients prevail. An upper bound to the erroneously allowed O_2 flux is the flux which (if only the P_{O_2} field of the RBC E_i is considered) would enter the space occupied by the adjacent RBCs and cfls. In our model the gap between two adjacent RBCs in one-half RBC length (as measured by Honig, personal communication), and for this situation the upper bound on the error is 10% of the total RBC O_2 flux. Considering that in the real situation P_{O_2} gradients between RBCs are predominantly directed away from the capillary, the bulk of the diffusive axial O_2 flux would be diverted to the tissue. (This latter effect has been quantified with a theoretical model of RBC O_2 unloading in capillaries for a slightly different geometry. Federspiel and Popel [1986] showed that at gaps of 0.5 RBC lengths the RBC O_2 flux is between 95 and 99% of maximum flux, which is the flux at infinite gaps, hence the one implicitly assumed in the present model.) Therefore one would guess that the above error amounts to no more than a few percent. For the situation presently studied, the only consequences of such an error in RBC O_2 flux would be that peri-erythrocytic P_{O_2} drops are by a few percent larger and that capillary P_{O_2} might be insufficient to supply the entire fiber with oxygen. Considering that effective capillary density in the model is still somewhat smaller than measured one (Honig and Odoroff, 1981), a moderate increase in P_{O_2} drops would not pose any serious problem. Apart from this effect, the characteristics of the calculated P_{O_2} fields will remain exactly as described (see above). If two RBCs are approaching each other even closer it may be preferable to model them as just one prolate spheroid.

Homogeneous O_2 consumption

(*a*) *Macroscale heterogeneities.* If the local consumption rate is given by some differentiable function $A(\vec{x})$, then Eq. 10 has to be replaced by

$$P_0^*(\vec{x}) = g(\vec{x}) - \frac{1}{4\pi}\int\int\int_{\mathcal{T}} \frac{A(\vec{u})}{\|\vec{x}-\vec{u}\|}\,du_x\,du_y\,du_z, \quad (26)$$

where g is an appropriately chosen harmonic function on $\mathcal{T}$ (see e.g., Bronstein and Semendjajew, 1981).

(*b*) *Microscale heterogeneities.* In RBCs and carrier-free layers the O_2 consumption rate is negligible as compared with myocytes. On the other hand, tissue O_2 consumption is not distributed homogeneously but takes place inside the mitochondria only. Clark and Clark (1985) have shown that P_{O_2} gradients introduced by such microscale heterogeneities are trivial. In the framework of the present model it is possible, however, to replace the term P_0^* in Eq. 9 which accounts for O_2 consumption, by a sum of terms, one for each oxygen consumer, in the same fashion as it was performed for the O_2 sources E_l. Each one of these terms would then be similar to the P_{O_2} field of an isolated mitochondrion as derived in Clark and Clark, 1985.

(*c*) *P_{O_2}-dependent O_2 consumption.* It is well known that O_2 turnover in mitochondria is practically independent of P_{O_2}, unless P_{O_2} drops to very low values of some tenths of a mmHg (Gayeski et al., 1987). Therefore the problem of considering P_{O_2}-dependent O_2 consumption may be reduced to turning off consumption if P_{O_2} falls to 0. The approach taken here to build up P_{O_2} distributions prohibits inclusion of a P_{O_2} dependence in the consumption term P_0^*. It is possible, however, during the iteration process for finding B_0 and C_{lT}, to identify anoxic regions within $\mathcal{T}$. For these regions $A(\vec{x})$ may be set to 0 if P_0^* is calculated according to Eq. 26. If the approach according to (*b*) is taken, mitochondria residing inside of these regions may be omitted from the summation for P_0^*.

P_{O_2} drops inside RBCs

P_{O_2} drops inside the erythrocytes are generally very small under physiological conditions; see Clark and Clark (1986). (Intra-erythrocytic P_{O_2} drops in the above application of the present model average 3.3 mmHg.) Therefore, they have been considered here by the first order approximation (Eq. 4) according to Clark and Clark (1986). If for some reason (high O_2 consumption rate, thin carrier-free layer, and high effective diffusivity) O_2 flux densities and hence intra-erythrocytic P_{O_2} drops become larger, the full analysis of RBC O_2 desaturation by Clark et al. (1985) may be utilized to obtain higher order expansions for $\bar{P}_{lE}$.

Linear RBC O_2 unloading

Between adjacent RBC positions, RBC O_2 flux is assumed to be a linear function of time. O_2 desaturation calculated for a constant P_{O_2} of 0 mmHg at the interface between carrier-free layer and tissue is roughly exponential with a half decay time of ~225 ms (Groebe and Thews, 1986). As transit times between adjacent RBC positions are only 4.3 ms in the application of the model, the time course of O_2 unloading can well be approximated by linear functions on time intervals of this length.

Constant surface P_{O_2} on E_l

For reasons of numerical tractability, RBC surface P_{O_2} is set to a constant value $\bar{P}_{lE}$ in reasonable agreement with the results of a two-dimensional numerical model for RBC O_2 desaturation in capillaries (Groebe and Thews, 1986). If one wanted to be more precise or if E_l is very long as in a vessel segment so that a decreasing surface P_{O_2} is expected, the longitudinal variation in surface P_{O_2} may be expressed by a series of Legendre polynomials (see Morse and Feshbach, 1953). In this case, the P_{O_2} fields P_l and P_l^* (Eq. 14) are functions of not only the prolate spheroidal coordinate ξ_l but also of η_l. For calculating the first order approximation to the mean surface P_{O_2}, $\bar{P}_{lE}$, Eq. 4 still can be used. Higher order approximations, however, require a more detailed analysis.

Equilibrium assumption in the tissue

O_2 and myoglobin are modeled to be in chemical equilibrium all over the tissue. From Fletcher's work (1980) who calculated equilibrium and nonequilibrium solutions in a Krogh cylinder model, it may be concluded that this is a reasonable assumption.

The author thanks Drs. G. Thews, A. Clark, and C. Honig for their many stimulating suggestions in the preparation of the manuscript.

Received for publication 3 April 1989 and in final form 13 November 1989

REFERENCES

Altman, P. L., and D. S. Dittmer. 1972. Biology Data Book. Federation of American Societies for Experimental Biology, Bethesda. 1850 pp.

Brodal, P., F. Ingjer, and L. Hermansen. 1977. Capillary supply of skeletal muscle fibers in untrained and endurance-trained men. *Am. J. Physiol.* 232:H705–H712.

Bronstein, I. N., and K. A. Semendjajew. 1981. Taschebuch der Mathematik. H. Deutsch Verlag, Thun, Switzerland. 553 pp.

Bruley, D. F. 1980. Probabilistic solutions and models: oxygen transport in the brain microcirculation. *In* Mathematics of Microcirculation Phenomena. J. F. Gross and A. Popel, editors. Raven Press, New York. 133–158.

Clark, A., and P. A. A. Clark. 1985. Local oxygen gradients near isolated mitochondria. *Biophys. J.* 48:931–938.

Clark, A., and P. A. A. Clark. 1986. The end-points of the oxygen path: transport resistance in red cells and mitochondria. *Adv. Exp. Med. Biol.* 200:43–47.

Clark, A., W. J. Federspiel, P. A. A. Clark, and G. R. Cokelet. 1985. Oxygen delivery from red cells. *Biophys. J.* 47:171–181.

Clark, P. A. A., S. D. Kennedy, and A. Clark. 1989. Buffering of muscle tissue P_{O_2} levels by the superposition of the oxygen field from many capillaries. *Adv. Exp. Med. Biol.* 248:165–174.

Egginton, S., Z. Turek, and L. Hoofd. 1987. Morphometric analysis of sparse capillary networks. *Adv. Exp. Med. Biol.* 215:1–12.

Federspiel, W. J. 1986. A model study of intracellular oxygen gradients in a myoglobin-containing skeletal muscle fiber. *Biophys. J.* 49:857–868.

Federspiel, W. J., and A. S. Popel. 1986. A theoretical analysis of the effect of the particulate nature of blood on oxygen release in capillaries. *Microvasc. Res.* 32:164–189.

Fenton, B. M., and B. W. Zweifach. 1981. Microcirculatory model relating geometrical variation to changes in pressure and flow rate. *Ann. Biomed. Eng.* 9:303–321.

Fletcher, J. E. 1978. Mathematical modelling in the microcirculation. *Math. Biosci.* 38:159–202.

Fletcher, J. E. 1980. On facilitated oxygen diffusion in muscle tissues. *Biophys. J.* 29:437–458.

Gayeski, T. E. J., and C. R. Honig. 1986. O_2 gradients from sarcolemma to cell interior in red muscle at maximal $\dot{V}_{O_2}$. *Am. J. Physiol.* 251:H789–H799.

Gayeski, T. E. J., and C. R. Honig. 1988. Intracellular P_{O_2} in long axis of individual fibers in working dog gracilis muscle. *Am. J. Physiol.* 254:H1179–H1186.

Gayeski, T. E. J., R. J. Connett, and C. R. Honig. 1987. Minimum intracellular P_{O_2} for maximum cytochrome turnover in red muscle in situ. *Am. J. Physiol.* 252:H906–H915.

Groebe, K., and G. Thews. 1986. Theoretical analysis of oxygen supply to contracted skeletal muscle. *Adv. Exp. Med. Biol.* 200:495–514.

Groebe, K., and G. Thews. 1989. Effects of red cell spacing and red cell movement upon oxygen release under conditions of maximally working skeletal muscle. *Adv. Exp. Med. Biol.* 248:175–185.

Grunewald, W. A., and W. Sowa. 1977. Capillary structures and O_2 supply to tissue. *Rev. Physiol. Biochem. Pharmacol.* 77:149–209.

Hellums, J. D. 1977. The resistance to oxygen transport in the capillaries relative to that in the surrounding tissue. *Microvasc. Res.* 13:131–136.

Homer, L. D., J. B. Shelton, C. H. Dorsey, and T. J. Williams. 1984. Anisotropic diffusion of oxygen in slices of rat muscle. *Am. J. Physiol.* 246:R107-R113.

Honig, C. R., and C. L. Odoroff. 1981. Calculated dispersion of capillary transit times: significance for oxygen exchange. *Am. J. Physiol.* 240:H196–H208.

Honig, C. R., M. L. Feldstein, and J. L. Frierson. 1977. Capillary lengths anastomoses, and estimated capillary transit times in skeletal muscle. *Am. J. Physiol.* 233:H122–H129.

Hoofd, L., Z. Turek, and J. Olders. 1989. Calculation of oxygen pressures and fluxes in a flat plane perpendicular to any capillary distribution. *Adv. Exp. Med. Biol.* 248:187–196.

Morse, P. M., and H. Feshbach. 1953. Methods of Theoretical Physics. McGraw-Hill Book Co., New York. 1284–1285.

Murray, J. D. 1974. On the role of myoglobin in muscle respiration. *J. Theor. Biol.* 47:115–126.

Popel, A. S. 1980. Mathematical modelling of convective and diffusive transport in the microcirculation. *In* Mathematics of Microcirculation Phenomena. J. F. Gross and A. Popel, editors. Raven Press, New York. 63–88.

Reeves, W. J., and K. Rakusan. 1987. Myocardial capillary flow pattern as determined by the method of coloured microspheres. *Adv. Exp. Med. Biol.* 222:447–453.

Riveros-Moreno, V., and J. B. Wittenberg. 1972. The self-diffusion coefficients of myoglobin and hemoglobin in concentrated solutions. *J. Biol. Chem.* 247:895–901.

Sarelius, I. H. 1986. Cell flow path influences transit time through striated muscle capillaries. *Am. J. Physiol.* 250:H899–H907.

Skalak, R., and P.-I. Branemark. 1969. Deformation of red blood cells in capillaries. *Science (Wash. DC).* 164:717–719.

Vaupel, P. 1976. Effect of percentual water content in tissues and liquids on the diffusion coefficients of O_2, CO_2, N_2, and H_2. *Pfluegers Arch. Eur. J. Physiol.* 361:201–204.

Wittenberg, J. B. 1970. Myoglobin-facilitated oxygen diffusion: role of myoglobin in oxygen entry into muscle. *Physiol. Rev.* 50:559–636.

Zander, R. 1975. Cellular oxygen concentration. *Adv. Exp. Med. Biol.* 75:463–467.